Journal of Neurochemistry

JOURNAL OF NEUROCHEMISTRY | 2010 | 115 | 1245–1255 doi: 10.1111/j.1471-4159.2010.07021.x

Conformational changes in extracellular loop 2 associated with signal transduction in the glycine receptor

Jennie M. E. Cederholm,*,† Nathan L. Absalom,‡,§,[1] Silas Sugiharto,* Renate Griffith,* Peter R. Schofield*,†,‡ and Trevor M. Lewis*

*School of Medical Sciences, The University of New South Wales, Sydney, New South Wales, Australia

†Neuroscience Research Australia, Randwick, New South Wales, Australia

‡Neurobiology Research Program, Garvan Institute of Medical Research, Sydney, New South Wales, Australia

§School of Medicine, The University of New South Wales, St Vincent's Hospital, Sydney, New South Wales, Australia

Abstract

Ligand-gated ion channels efficiently couple neurotransmitter binding to the opening of an intrinsic ion channel to generate the post-synaptic potentials that are characteristic of fast synaptic transmission. In the Cys-loop family of ligand-gated ion channels, the ligand-binding site is approximately 60 Å above the channel gate. Structural modelling of related proteins and mutagenesis studies led to the hypothesis that loops 2 and 7 of the extracellular domain may couple ligand binding to receptor activation. Mutating loop 2 residues of the glycine receptor to cysteine reveals an alternating pattern of effect upon receptor function. Mutations A52C, T54C and M56C produced a threefold right-shift in EC_{50}. In contrast, a 30-fold right-shift was seen for mutations E53C, T55C and D57C. Loop 2 conformational changes associated with ligand binding were assessed by measuring the rate of covalent modification of substituted cysteines by charged methane thiosulfonate reagents. We show for the first time state-dependent differences in the rate of reaction. A52C and T54C are more accessible in the resting state and M56C is more accessible in the activated state. These results demonstrate that loop 2 does undergo a conformational change as part of the mechanism that couples ligand binding to channel opening.

Keywords: channel gating, extracellular domain, Glycine receptor, loop 2, signal transduction.

J. Neurochem. (2010) **115**, 1245–1255.

The glycine receptor (GlyR) is a member of the Cys-loop family of ligand-gated ion channels (LGICs) that includes the nicotinic acetylcholine receptor (nAChR), serotonin type 3 receptor (5-HT_3R) and GABA type A receptor. Each of these receptors is a pentameric complex, with the subunits arranged around a central ion-conducting pore within the cell membrane (Betz 1990). The individual subunits share a common topology with a large extracellular domain (ECD) at the N-terminus and four transmembrane domain α-helices (M1–M4), of which M2 lines the channel pore. The ECD is composed predominantly of β-sheets arranged in a β-sandwich, with six strands forming the outer β-sheet and four strands forming the inner β-sheet based upon homology with the acetylcholine binding protein (AChBP; Brejc *et al.* 2001). The stretches of residues that link β-strands are referred to as loops. The ligand binding site is located in the ECD at the interface of adjacent subunits and is spatially distant from the channel gate (~ 60 Å) located in the transmembrane domain (Unwin 1993; Lynch 2004). Given the separation of the ligand binding site from the gate, there needs to be communication between these sites to allow opening of the channel in response to ligand binding.

The interface between the ECD and the transmembrane domain is an important element in coupling ligand binding to channel opening. The crystal structure of the AChBP (Brejc *et al.* 2001) led to the hypothesis that loops, such as loop 2 between β-strands β1 and β2 of the inner sheet, are

Received May 14, 2010; revised manuscript received August 26, 2010; accepted September 17, 2010.

Address for correspondence and reprint requests to Trevor M. Lewis, School of Medical Sciences, The University of New South Wales, UNSW Sydney, NSW 2052, Australia. E-mail: t.lewis@unsw.edu.au

[1]The present address of Nathan L. Absalom is the Faculty of Pharmacy, University of Sydney, NSW 2006, Australia.

Abbreviations used: 5-HT_3R, serotonin type 3 receptor; AChBP, acetylcholine binding protein; ECD, extracellular domain; ELIC, *Erwinia chrysanthemi*; GLIC, *Gloeobacter violaceus*; GlyR, glycine receptor; LGICs, ligand-gated ion channels; MTS, methane thiosulfonate; MTSES, 2-sulfonatoethyl methanethiosulfonate; MTSET, 2-(trimethylammonium)ethyl methanethiosulfonate; nAChR, nicotinic acetylcholine receptor.

in a position to link these two functional domains (Dougherty and Lester 2001; Lester *et al.* 2004). A chimera between the AChBP and the transmembrane domain of the 5-HT_{3A}R was only functional when residues within three loops of the AChBP were mutated to the corresponding residues of the 5-HT_{3A}R loops (Bouzat *et al.* 2004). This work highlighted the role that these loops, including loop 2, play in the functional coupling of the ligand binding domain and the channel pore.

Comparison of the *Torpedo* nAChR structure and the atomic structure of the AChBP also implies that loop 2 is important for receptor activation (Unwin *et al.* 2002; Unwin 2003). This comparison revealed differences between the α and non-α subunits. It is suggested that the α subunits have a 'distorted' conformation in the resting state, which is probably because of interactions with neighbouring subunits. Ligand binding somehow overcomes this distortion, allowing the α subunits to relax and switch to the non-α conformation so that the receptor adopts a more symmetrical structure. The conformational change of the α subunit is possibly because of the relative movements of the inner and outer β-sheets of the ECD around the conserved disulfide bridge. Thus, upon ligand binding the inner β-sheet of the α subunit is predicted to rotate ∼ 10° clockwise about an axis oriented normal to the membrane plane (Unwin 2005). The movement of the inner β-sheet, including loop 2, is expected to contribute to the mechanism that triggers opening of the channel pore.

Movement of loops in the ECD during receptor activation has also been inferred from comparison of the crystal structures of two prokaryotic LGICs: *Erwinia chrysanthemi* (ELIC) – which is presumed to be in the closed state (Hilf and Dutzler 2008) and *Gloeobacter violaceus* (GLIC) – which is presumed to be in the open state (Bocquet *et al.* 2009; Hilf and Dutzler 2009). Comparing these structures reveals that the receptor appears to undergo a concerted quaternary twist, with the ECD rotating in an anticlockwise direction and the transmembrane domain rotating in a clockwise direction (Bocquet *et al.* 2009; Corringer *et al.* 2010), as it progresses from the closed to the open state. Each subunit also appears to undergo a tertiary twist with the entire core of the β-sandwich rotating clockwise (∼ 8°) around an axis that is approximately parallel to the inner β-sheet. The movement of the inner β-sheet may lead to the downward motion of loop 2 (β1–β2) towards the pore and tilting the M2–M3 loop away from the central axis. These conformational changes are predicted to contribute to opening the channel pore.

In this study, we tested for the suggested conformational change in loop 2 of the α1 GlyR by assessing the availability of substituted cysteine residues in loop 2 for covalent modification. Here, we demonstrate, for the first time, state-dependent differences in the structure of loop 2, which we propose are intimately involved in the coupling of ligand binding to opening of the channel pore.

Materials and methods

Molecular modelling

During this work two crystal structures of prokaryotic LGICs were published, ELIC and GLIC. Along with the refined structure of the *Torpedo* AChR that was published in 2005 (Unwin 2005) three homology models of the GlyR α1 subunit were made using these structures. Chains A to E of ELIC (PDB accession no. 2VLO) (Hilf and Dutzler 2008), GLIC (PDB accession no. 3EAM) (Bocquet *et al.* 2009) or *Torpedo* (PDB accession no. 2BG9) (Unwin 2005) were separately aligned with the GlyR α1 subunit sequence using ClustalW. Full alignments are provided in Appendix S1 (Figure S1). The alignments were then individually put into the web-based Swiss-Model Workspace (Schwede *et al.* 2003) to model the GlyR α1 subunits. The five subunit models from each crystal structure were then merged into a pentameric structure using the DeepView software (Guex and Peitsch 1997) and refined by removing clashes (http://www.expasy.org./spdbv/). The models were then imported into the Discovery Studio software (version 2.5; DS2.5) by Accelrys (http://accelrys.com/). Hydrogens were added, the C-terminal residues after V307 and the N-terminal residues before P36 were deleted, and the termini of all chains were set to neutral. It should be noted that deletion of these regions does not interfere with the receptor structure as a whole or the loop of interest. Atoms were typed with the CHARMm force field as implemented in DS2.5. Two rounds of energy minimisations were carried out. First, all heavy atoms were fixed and the hydrogens minimised to convergence (root-mean-square gradient < 0.1 kcal/M/Å). Second, the backbone was fixed, and the side-chains minimised to convergence (root-mean-square gradient < 0.1 kcal/M/Å). For the determination of % surface accessibility of each loop 2 residue the minimised models were imported back into DeepView. Further details on molecular modelling are provided in Appendix S1.

Mutagenesis and expression of human GlyR α1 subunit cDNA

The cDNA encoding the wild-type human α1 subunit of the GlyR was subcloned into the pCIS expression vector. Site-directed mutagenesis was performed using the oligonucleotide-directed PCR technique and confirmed by DNA sequencing of the complete plasmid. To ensure that the sulfhydryl reagents only reacted with the substituted cysteine residues, we used receptor subunits in which the free cysteine residue at position 41 in the extracellular domain had been mutated to an alanine (Lynch *et al.* 2001). All of the substituted cysteine mutations were introduced on this α1(C41A) background. Exponentially growing 293 cells (ATCC CRL 1573) were transiently transfected using the polymer-based DNA transfection reagent jetPEI according to the manufacturer's instruction (Polyplus-transfection, Illkirch, France). Wild-type or mutated α1 subunits of the human GlyR along with cDNA for the CD4 protein (2 : 1, α1 GlyR : CD4) was mixed with the appropriate amount of jetPEI calculated for a N/P ratio of 5. Transfected cells were identified by labelling with CD4 polystyrene beads (Dynabead M-450, CD-4; Dynal, Great Neck, NY, USA).

Electrophysiology

Using standard patch-clamp techniques, whole-cell currents were recorded in response to the application of glycine with a modified

U-tube (exchange time of 10 ms). All experiments were performed at 21 ± 1°C. The cells were continually superfused with an external bathing solution containing (mM): 140 NaCl, 5 KCl, 2 $CaCl_2$, 1 $MgCl_2$, 10 HEPES and 10 glucose, adjusted to pH 7.4 with NaOH. Glycine concentrations were made up in the external bathing solution. Patch pipettes were fabricated from borosilicate glass capillaries and fire polished to give a tip resistance of 2–6 MΩ. Pipettes were filled with an intracellular solution containing (mM): 120 CsCl, 20 TEACl, 2 $MgCl_2$, 10 HEPES and 11 EGTA adjusted to pH 7.2 with CsOH. Whole-cell currents were recorded at a holding potential of −50 mV using either an Axopatch-1D or Axopatch-200B amplifier and digitised using pClamp 10.0 software and either a Digidata 1200 ADC interface or a Digidata 1440A (Molecular Devices, Union City, CA, USA). At least 80% series resistance compensation was achieved in each experiment. Concentration-response curves were constructed from the peak current response to the application of a range of agonist concentrations, with a minimum of one minute between successive applications.

Sulfhydryl reagents and rates of reaction

Substituted cysteine mutations were introduced one at a time in the α1 GlyR at positions 51–57 inclusive, in loop 2 of the extracellular domain. Each of these mutants was assessed for covalent modification with methane thiosulfonate (MTS) derivatives applied directly to the cell in the presence or absence of agonist. We chose to use the negatively charged 2-sulfonatoethyl methanethiosulfonate (MTSES) and the positively charged 2-(trimethylammonium)ethyl methanethiosulfonate (MTSET) (Toronto Research Chemicals Inc. North York, Ontario, Canada). Stock solutions of 100 mM MTSES and MTSET in distilled water were aliquotted into screw-cap microcentrifuge tubes and rapidly frozen in an ethanol/dry ice mix before storage at −20°C. For each application of MTS reagents, a new aliquot was thawed, diluted in bathing solution to the working concentration (100 μM) and used immediately.

The rate of covalent modification of cysteine substituted GlyRs by MTS reagents was measured in the presence and absence of glycine. Rates determined in the absence of glycine are assumed to reflect the resting conformation of the receptor. Co-application of MTS reagents with a saturating concentration of glycine is expected to drive the receptor equilibrium towards the activated conformation of the receptor. The amplitude of the current in response to a concentration of glycine eliciting a 30% response (I_{30}) and a maximum concentration of glycine (I_{max}) were recorded at least three times prior to MTS reagent addition. For reactions in the activated state, 100 μM MTSES or 100 μM MTSET was co-applied with a saturating concentration of glycine (20 mM) for a duration of 2 s on successive occasions, interleaved with test applications of glycine at the same concentration that elicited the initial I_{30} and I_{max} responses. These test applications were used to determine any changes in the I_{30} and I_{max} responses. The I_{30} and I_{max} responses at successive cumulative time points were normalised to the responses recorded prior to MTS application. Reactions in the resting state were similarly determined, except the 100 μM MTSES or 100 μM MTSET was applied in the absence of glycine. The data sets obtained in this way were fitted with a single exponential decay (Sigmaplot®, Systat Software Inc., San Jose, CA, USA) to obtain an estimate of the second order rate constant, using the following equation:

$$I_t = I_\infty - (I_\infty - I_0).e^{-\kappa.[M].t}$$

where I_0 is the initial response, I_t is the normalised response at each cumulative time point, t, with [M] the concentration of MTS reagent applied. The estimated parameters are the response at the end of the reaction, I_∞, and the second order rate constant, κ. The average second order rate constant was determined from at least three separate cells.

Data analysis and statistics

Concentration-response data were plotted on semi-logarithmic axes and fitted using a non-linear least squares routine (Sigmaplot®, Systat Software Inc.) with the empirical Hill equation:

$$I = I_{max}\left(\frac{[A]^{n_H}}{[A]^{n_H} + EC_{50}^{n_H}}\right)$$

where I is the peak whole-cell current recorded following application of a range of concentrations of the agonist, [A]; I_{max} is the estimated maximum current, EC_{50} is the glycine concentration required for a half-maximum response and n_H is the Hill co-efficient.

Statistics (Systat Software Inc.) were performed on wild-type and mutant EC_{50} values using a one-way ANOVA on Ranks test. Second-order rate constants were compared using unpaired t-tests comparing activated and resting states.

Results

We employed substituted cysteine accessibility method to assess the function and conformational changes of loop 2 in the ECD of the α1 GlyR (Karlin and Akabas 1998). The availability of substituted cysteines in loop 2 for covalent modification was assessed in the resting state and the activated state using the negatively charged MTSES and positively charged MTSET reagents. First, it was necessary to determine the effects of the mutations on receptor function.

Effects of mutations to cysteine

To eliminate the possibility of MTS reagents reacting with the cysteine residue at position 41 (C41) in the ECD, all mutant receptors were constructed on an α1(C41A) background. We have previously shown that the α1(C41A) receptor has concentration-response characteristics indistinguishable from the wild-type and is unchanged following application of 500 μM MTSES or 500 μM MTSET for 1 min (Absalom *et al.* 2003).

Concentration-response curves were produced for each of the cysteine mutants in loop 2 (I51C, A52C, E53C, T54C, T55C, M56C and D57C) to assess the impact of each mutation upon GlyR activation (Fig. 1). Six mutants resulted in receptors that produced glycine-evoked currents when expressed in HEK293 cells, with the I51C mutant failing to

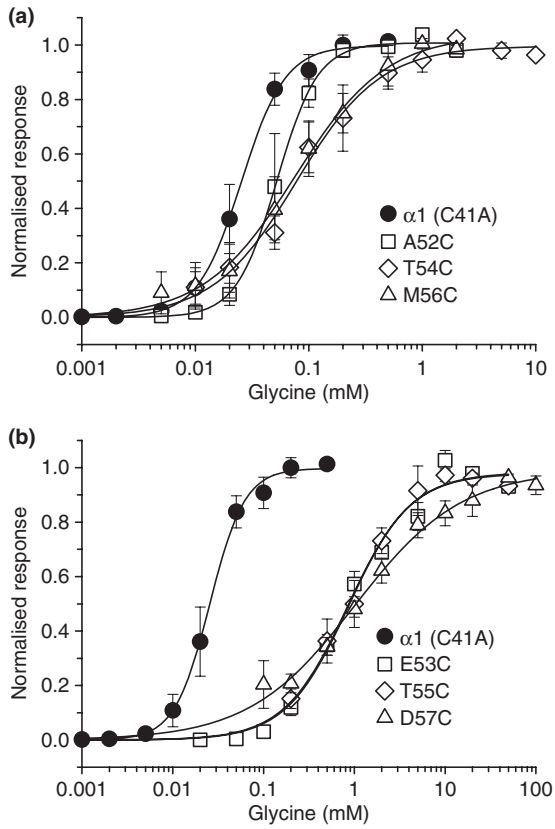

Fig. 1 Concentration response curves of α1(C41A) and loop 2 substituted cysteine α1 homomeric GlyRs. Concentration response curves are shown for the (a) α1(C41A) wild-type background (*filled circles*), A52C (*open squares*), T54C (*open diamonds*), M56C (*open triangles*), (b) α1(C41A) wild-type background (*filled circles*), E53C (*open squares*), T55C *(open diamonds*), and D57C (*open triangles*) mutant receptors. Each data point represents the mean ± SEM; $n = 5$. The fitted curves obtained with the Hill equation are shown as solid lines.

Table 1 Effects of substituted cysteine mutations

	I_{max}	EC_{50}	ΔEC_{50}		
Mutant	nA	μM	fold-change	n_H	*n*
C41A	9.2 ± 1.5	27 ± 4	–	2.75 ± 0.3	5
I51C	–	–	–	–	4
A52C	11 ± 1.6	51 ± 10	1.8	2.46 ± 0.14	5
E53C	3.7 ± 1.9	920 ± 70*	33	1.27 ± 0.12	5
T54C	5.0 ± 3.2	87 ± 40	3.2	1.38 ± 0.21	4
T55C	1.3 ± 0.7	780 ± 230*	29	1.34 ± 0.13	5
M56C	3.1 ± 1.3	89 ± 30	3.3	1.58 ± 0.17	5
D57C	0.02 ± 0.01	1080 ± 200*	40	0.88 ± 0.13	5

All values are the mean ± SEM of each parameter obtained from the fit of the Hill equation to each data set. All values for the α1(C41A) GlyR and part of the dataset for the E53C and D57C concentration-response curves are reproduced from Absalom *et al.* (2003). Displayed are values for maximal current (I_{max}), half-maximal activation (EC_{50}), Hill coefficient (n_H) and number of experiments (*n*). The fold-change in EC_{50} (ΔEC_{50}) is relative to the EC_{50} value obtained for α1(C41A) GlyR. The I_{max} and EC_{50} of the α1(C41A) GlyR is not significantly different to the wild-type GlyR (Lynch *et al.* 2001). I51C produced no glycine-evoked currents. Values accompanied by an asterisk (*) are significantly different to that of the α1(C41A) GlyR (*$p < 0.05$).

show glycine-evoked currents, even with glycine applied at concentrations of up to 10 mM. Examples of whole-cell currents recorded for each mutant are provided in Appendix S1 (Figure S2). The mutants A52C, T54C and M56C, at alternating positions along loop 2, all exhibited small increases in the EC_{50} for glycine (at most a 3.3-fold increase) in comparison with the α1(C41A) receptor (Fig. 1a, Table 1). Interestingly, in oocytes the concentration-response curve of T54C is shifted to the left (Crawford *et al.* 2008) compared to the modest shift to the right in our study. We suggest that this difference is because of the different expression systems. Conversely, the E53C, T55C and D57C receptors all exhibited at least a 29-fold increase in the EC_{50} (Fig. 1b, Table 1). The average maximum whole-cell current was also decreased by at least ∼ twofold for the six mutants. This decrease was most dramatic at D57C mutant receptors, where the whole-cell current was reduced by 460-fold compared to the α1(C41A) receptor (Table 1). A marked decrease in the Hill slope was also observed for the mutants, with the exception of A52C. Given that loop 2 is approximately 40 Å away from the ligand binding domain, these changes in Hill slope, EC_{50} and I_{max} are together indicative of an impairment in the signal transduction mechanism of the receptor (Colquhoun 1998). This is consistent with previous data on loop 2 demonstrating a role in signal transduction in the GlyR (Absalom *et al.* 2003; Plested *et al.* 2007; Pless and Lynch 2009b), and other pentameric LGICs (Kash *et al.* 2003; Reeves *et al.* 2005). The lack of glycine-evoked currents with mutant I51C suggests that I51 may be critically important for protein assembly and/or gating, although this mutation has been successfully expressed in oocytes with a maximum current approximately 50% of the wild-type receptor (Crawford *et al.* 2008).

Effects of MTS reagents on introduced cysteines

Each of the functional cysteine mutants was assessed for accessibility to MTS reagents for covalent modification. Glycine concentration-response curves were generated and MTSES or MTSET reagents were then applied for 5 min at a single concentration (500 μM). The consequences of reaction with MTSES or MTSET were then determined with the application of glycine concentrations that had elicited a maximum response (I_{max}) and a response approximately 30% of maximum (I_{30}) prior to MTS reaction. Only T54C and M56C showed any change in response following application of MTSES. The M56C receptor showed a threefold increase

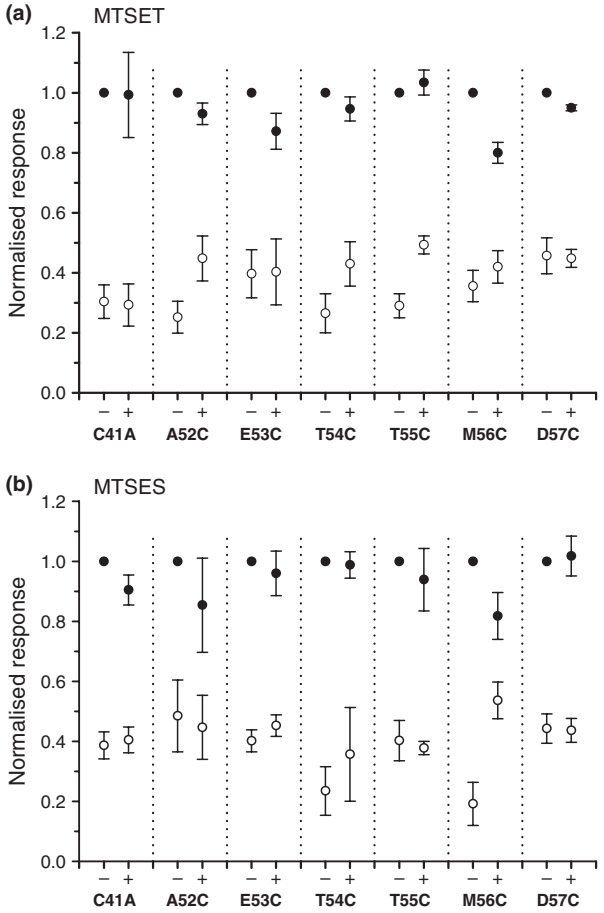

Fig. 2 The effects of MTS reagents on α1(C41A) and loop 2 substituted cysteine α1 homomeric GlyRs. (a) The I_{30} (*open circles*) and I_{max} (*closed circles*) responses before (–) and after (+) MTSET reagent addition for each of the mutants in loop 2 and the α1(C41A) receptor; (b) The I_{30} and I_{max} response before (–) and after (+) MTSES reagent addition for each of the mutants in loop 2 and the α1(C41A) receptor. Each data point represents the mean ± SEM; n = 3–11.

in the I_{30} response and a 20% reduction in the I_{max} response, while T54C showed a small 1.5-fold increase in the I_{30} response (Fig. 2b). In contrast, after addition of MTSET, the mutants A52C, T54C and T55C each showed approximately a 1.7-fold increase in the I_{30} response, without any change in the I_{max} response (Fig. 2a). The M56C mutant exhibited an 18% reduction in the I_{max} response following application of MTSET, but there was no alteration in the I_{30} response. The remaining mutants, E53C and D57C, exhibited no change in either the I_{30} or I_{max} responses, suggesting that they were not modified by MTSET or that there was no functional effect following MTSET modification.

Rate of reaction of MTS reagents

Those loop 2 cysteine substitutions that were identified as being accessible for covalent MTS modification (A52C, T54C, T55C, M56C) were investigated further for agonist-dependent changes in accessibility. The rate of reaction for MTS modification was determined from repeated applications of MTS reagents in the presence and absence of glycine. MTS reagents are known to react 5×10^9 times faster with cysteines on the water-accessible surface of the protein where they can be deprotonated to a thiolate (S^-), compared with the protonated thiol that is less likely to be water-accessible (Karlin and Akabas 1998). The measurement of the rate constants allows inferences to be made about agonist-dependent conformational changes (Pascual and Karlin 1998). MTS reagents were applied for 2 s alone (resting state) or in the presence of a saturating concentration of glycine (20 mM; activated state). In between MTS applications, currents activated by ~ EC_{30} concentration of glycine were recorded. Normalised changes in the I_{30} response were plotted against the cumulative application time to determine the rate constant of the reaction. Two examples of such experiments are shown in Fig. 3 for the reaction of A52C with MTSET and T54C with MTSES. The rate of reaction with MTSES determined for the M56C receptor, was eightfold slower in the resting state (1200/M/s) than the activated state (10 000/M/s; $p = 0.002$; Figs 4 and 6b, Table 2). Interestingly, the rate of reaction of the T54C receptor with MTSES was 1.7-fold faster in the resting state (9100/M/s) than the activated state (5400/M/s; $p = 0.001$; Figs 4 and 6a, Table 2). For T54C, the rate of reaction with MTSET was not significantly different in the resting state (3900/M/s) compared with the activated state (3300/M/s; Figs 4 and 5b, Table 2). These rates were similar to those obtained for T55C (Fig. 5c) and are moderately slow when compared to rates obtained for some other mutants. In contrast, the rate of reaction for MTSET with the A52C receptor was sixfold faster in the resting state (6900/M/s) than in the activated state (1200/M/s; $p < 0.001$; Figs 4 and 5a, Table 2), indicating a clear difference in the environment around this residue between the resting and activated states. Overall, these results suggest that A52C and T54C are more accessible in the resting state and the M56C residue is more accessible after the transition to the activated state.

Analysis of glycine receptor homology models

Our models were checked against the structure templates to determine the fit between the structures. For a detailed description see Appendix S1.

Surface accessibility of loop 2 residues was calculated for the GlyR homology models using the DeepView software (see Appendix S1). For the GlyR homology model based on the prokaryotic ELIC structure we found that the most accessible residue is T54 closely followed by I51 and T55 (Table 3). Residue A52 is approximately 15–20% less accessible than these three residues, followed by M56 and D57. The conserved glutamate, E53, is the least accessible.

The GlyR homology model based on GLIC differs slightly to the model based on ELIC. In this model, T55 is the most

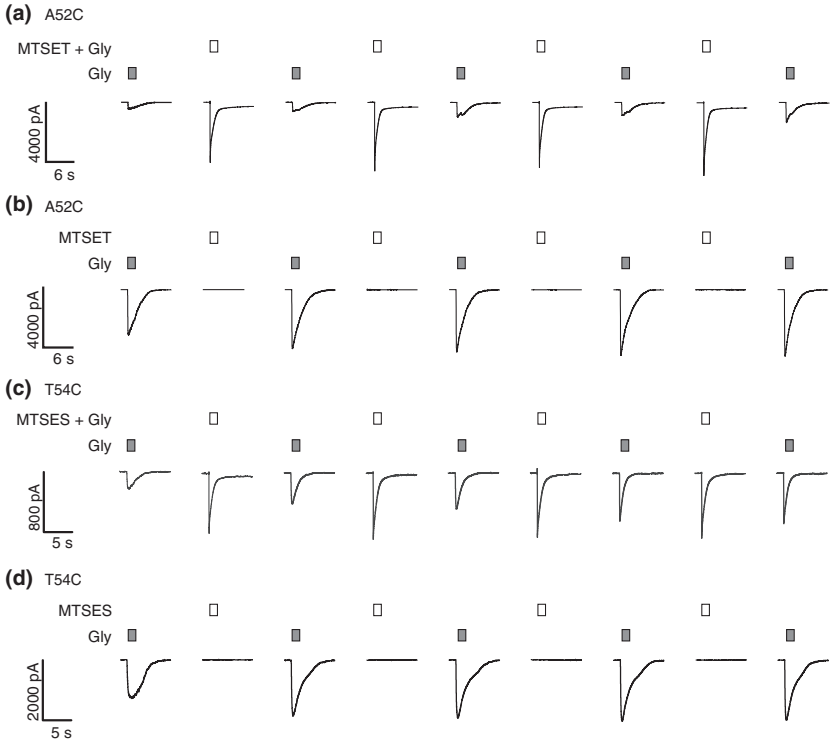

Fig. 3 The rate of reaction of MTS reagents with the A52C and the T54C GlyRs. An example of an experiment to determine the rate of reaction in the activated and resting states of A52C with MTSET (a and b, respectively) and T54C with MTSES (c and d, respectively) is shown. The amplitude of the whole-cell current response to a concentration of glycine eliciting a 30% response (I_{30}) and a maximum concentration of glycine (I_{max}) were recorded at least three times prior to the addition of the MTS reagent (current traces not shown). This glycine I_{30} dose was subsequently used as a test application (*grey bars*). For reactions in the activated state, 100 μM MTSET (a) or MTSES (c) was co-applied with a saturating concentration of glycine (20 mM) (*open bars*) for a duration of 2 s on successive occasions. These applications were interleaved with test applications of glycine (*grey bars*). The same protocol was used for reactions in the resting state (b and d). However, 100 μM MTSET or MTSES was applied in the absence of glycine. For both receptors, the amplitude of the I_{30} response increased over the time course of the experiment following application of the MTS reagent in both the resting and activated states.

accessible residue (28%) very closely followed by T54 (25%) (Table 3), while A52 is just slightly more accessible than I51 (19% and 17%, respectively). Surprisingly, E53 seems to be more accessible than both M56 and D57, with M56 calculated to be the least accessible of the two (Table 3).

As for the GlyR homology model based on *Torpedo*, T55 is the most accessible residue (35%; Table 3), surprisingly followed by M56. According to the calculations, M56 has 10% more of its surface accessible in the *Torpedo* model compared to the models based on ELIC and GLIC. M56 is followed by T54, D57 and I51. Also surprising is A52, which only has 4% of its surface accessible making it the second least surface accessible residue just before E53.

Discussion

We studied seven cysteine mutations in loop 2 of the ECD of the human α1 GlyR. This work complements and extends previous studies investigating the role of loop 2 charged residues in the activation of the α1 GlyR (Absalom *et al.* 2003) and more generally across other Cys-loop receptors (Kash *et al.* 2003; Lee and Sine 2005). In this study, we provide an insight into the structure and the conformational change of loop 2 in the GlyR by assessing the rate of modification of the introduced cysteines using MTS reagents.

Structure and functional changes of loop 2

In agreement with previous studies, loop 2 cysteine mutations produced an intriguing alternating pattern of functional changes to the α1 GlyR (Crawford *et al.* 2008). Large increases in glycine EC_{50} values were observed for E53C, T55C and D57C compared with the control α1(C41A) GlyR. Mutation of the intervening residues (A52C, T54C and M56C) all produced minor changes in the concentration-response curves. Our MTS reactivity data reinforces this pattern, as both E53C and D57C were not accessible for MTS modification, while A52C, T54C and M56C all exhibited state-dependent changes in the MTS rate constants. Together, this suggests that residues at

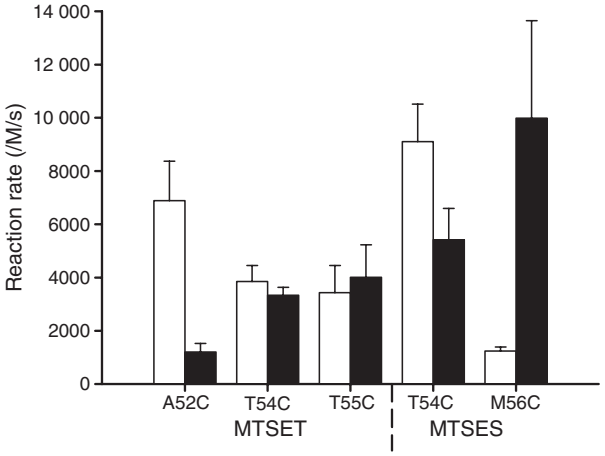

Fig. 4 The rates of reaction with MTSES and MTSET in the resting and activated states. The time constant for the second order rate of 100 μM MTSES or MTSET are given for each of the cysteine mutations in the resting state (*white bars*) and the activated state (*black bars*). Mutant A52C show a significant difference in the rate of reaction to 100 μM MTSET with the mutant receptor reacting faster to MTSET in the resting state. In contrast, mutants T54C and M56C show a significant difference in the rate of reaction to 100 μM MTSES. Similar to A52C, the T54C receptor reacts faster to MTSES in the resting state, while M56C reacts faster to MTSES in the activated state. Each vertical bar represents the mean ± SEM; n = 3–7.

positions 53, 55 and 57 are critical to the signal transduction and are likely to interact with other elements of this process.

A similar pattern of large shifts in EC_{50} values at alternating positions has also been described for cysteine substitutions in loop 2 of the α7 nAChR (McLaughlin *et al.* 2007). This implies that there may be a common structural motif shared between loop 2 of the α7 nAChR and the α1 GlyR. However, a full sequence alignment of these two receptor subunits does not result in a corresponding alignment of the loop 2 residues exhibiting a large shift in EC_{50} values (Fig. 7; see also Crawford *et al.* 2008). Displacement of the alignment by one residue in the N-terminal direction (Crawford *et al.* 2008) aligns the alternating pattern of EC_{50} values but we find no correlation of accessibility or rates of reaction. For example, displacement of α1 GlyR would align T54C with N46 in the α7 nAChR, and while T54C exhibits state-dependent changes in MTS reaction rate, N46C is not modified by MTS. One interpretation is that this may reflect differences in the molecular interactions of loop 2 with surrounding structures in the α7 nAChR compared to the α1 GlyR, perhaps because of differences in the packing of the ECD structure in these receptors.

We determined the relative percentage of surface accessibility of each loop 2 residue in the GlyR homology models as a guide to the steric hindrance that MTS reagents might experience. The subset of substituted cysteines that are modified by MTS reagents largely corresponds with those substitutions showing small shifts in the glycine EC_{50} values (A52C, T54C and M56C). Of the loop 2 residues, T54 and T55 show the highest overall accessibility (25–36%; Table 3), which is perhaps not surprising as these residues are predicted to form the apex of the loop and face the pore vestibule (Fig. 8). However, these residues are not equally accessible, with T54 predicted to be more accessible in the 'closed state' (36%) compared to the 'open state' (25%), and T55 showing virtually no difference in accessibility between these states (27% and 28%, respectively). These data are consistent with the MTSES reaction being faster in the resting state for T54C, and the state-independent reactions of MTSET observed for T55C. The lack of state-dependence of MTSET reactions at T54C suggests that local electrostatic influences may hinder the access of positively charged MTSET and favour the negatively charged MTSES in the resting state.

Our models predict that M56 faces towards loop 7 (Fig. 8), with little difference in accessibility of this residue between the GLIC ('open') and ELIC ('closed') homology models (~ 10%; Table 3). However, M56C clearly shows a faster reaction with MTSES in the activated state. Inspection of the models show M56 can be accessed from the protein

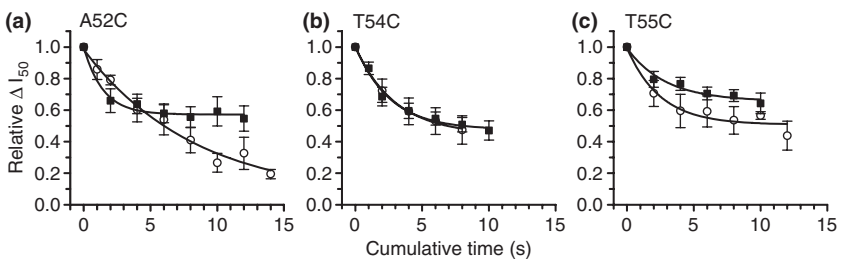

Fig. 5 The rates of reaction with MTSET with the A52C, T54C and T55C GlyR. Data were collected as described in Fig. 3. The mean data for the time course of reaction to MTSET is shown here for (a) A52C, (b) T54C and (c) T55C. Resting state is indicated by *filled squares* and the activated state by *open circles*. Currents are normalised to the response prior to MTSET addition and plotted against cumulative reaction time. Each set of data were fitted with a single exponential. The mean time constants in the resting state and the activated state for each mutant are shown in Table 2. Each data point represents the mean ± SEM; n = 3–11.

Table 2 Rate of reaction (κ) for MTS modification in the open and closed states

	Open state (+Gly)		Closed state (−Gly)	
Mutant	κ (/M/s)	*n*	κ (/M/s)	*n*
100 μM MTSET				
A52C	1200 ± 300	5	6900 ± 1500*	6
T54C	3300 ± 300	6	3900 ± 600	4
T55C	4000 ± 1200	5	3400 ± 1000	5
100 μM MTSES				
T54C	5400 ± 1200	7	9100 ± 1400*	5
M56C	10 000 ± 3700	3	1200 ± 200*	5

All values are the mean ± SEM of each parameter obtained from the fit of a first order exponential decay curve. Displayed are values for the second order rate constant (κ) and number of experiments (*n*). The values of the closed state accompanied by an asterisk (*) are significantly different to that of the open state (*$p < 0.05$).

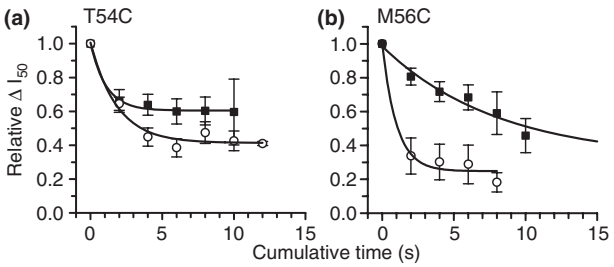

Fig. 6 The rates of reaction with MTSES with the T54C and M56C GlyR. Data were collected as described in Fig. 3. The mean data for the time course of reaction to MTSES is shown here for (a) T54C and (b) M56C. Resting state is indicated by *filled squares* and the activated state by *open circles*. Currents are normalised to the response prior to MTSES addition and plotted against cumulative reaction time. Each set of data were fitted with a single exponential. The mean time constants in the resting state and the activated state for each mutant are shown in Table 2. Each data point represents the mean ± SEM; *n* = 3–7.

surface outside of the pore vestibule, at the interface between adjacent subunits. It is possible that GLIC and ELIC are not good templates for the subunit interface of the α1 GlyR since they exhibit a much tighter packing of the subunits compared to the *Torpedo* structure and so may underestimate the accessibility.

Neither E53C nor D57C showed any change in function following reaction with MTSES or MTSET, which is in general agreement with the predicted low surface accessibility of E53 (1–13%) and D57 (10–14%) (Table 3). However, in oocytes the reaction of MTSES (but not MTSET) shifts the EC_{50} of E53C α1 GlyR to the left towards wild-type values (Crawford *et al.* 2008). In contrast, when 2-aminoethyl methanethiosulfonate is applied to the equivalent mutation in the α7 nAChR (E44C), the EC_{50} is shifted about twofold to

Table 3 Surface accessibility of seven loop 2 residues

	% surface accessibility		
Residue	'Closed state' (ELIC)	'Open state' (GLIC)	*Torpedo*
I51	29	17	12
A52	15	19	4
E53	9	13	1
T54	36	25	18
T55	27	28	35
M56	10	8	21
D57	10	11	14

Percentage surface accessibility in chain A, as determined using DeepView (for a detailed method description see Appendix S1), of the three homology models based on the prokaryotic crystal structures ELIC and GLIC, and the refined cryo-electron microscopy structure of the *Torpedo* nAChR. The 'Closed state' refers to our homology model based on ELIC, while the 'Open state' refers to our homology model based on GLIC.

Receptor	Loop 2											PDB
				i			*i*+3					
m nAChR α1	50	N	V	D	E	V	N	Q	I	V	T	59 2QC1
Tm nAChR	50	N	V	D	E	V	N	Q	I	V	E	59 2BG9
p ELIC	25	G	V	N	T	L	E	Q	T	Y	K	24 2VL0
p GLIC	29	S	L	D	D	K	A	E	T	F	K	38 3EAM
h GlyR α1	50	S	I	A	E	T	T	M	D	Y	R	59
c nAChR α7	41	D	V	D	E	K	N	Q	V	L	T	50

Fig. 7 Alignment of loop 2 sequences from LGICs. Shown here are the loop 2 sequences from the mouse nAChR (Dellisanti *et al.* 2007), the *Torpedo* nAChR (Unwin 2005), ELIC (Hilf and Dutzler 2008) and GLIC (Bocquet *et al.* 2009), for which there are structures available. Also shown are the α1 GlyR and the α7 nAChR (McLaughlin *et al.* 2007) sequences which have been probed for MTS accessibility. Residues that are part of a Type I beta turn are shown within the box. The positions of these residues in the beta turn are, from left to right, *i*, *i* + 1, *i* + 2 and *i* + 3. Residues showing a large shift in EC_{50} when mutated to cysteine are highlighted in grey, with I51 in the α1 GlyR based on the results from Crawford *et al.* (2008). Abbreviations: m, mouse; Tm, *Torpedo marmorata*; p, prokaryote; h, human; c, chick PBD, protein data bank accession identifier.

the right (McLaughlin *et al.* 2007). The equivalent glutamate residue in the α1 nAChR (Lee and Sine 2005) and the GABA type A receptor (Price *et al.* 2007; Wang *et al.* 2007) forms a salt bridge with a conserved arginine residue in the pre-M1 segment that is important for receptor gating, but not in the 5-HT_{3A}R (Price *et al.* 2007). Thus, while this residue is likely to play a role in receptor gating, the reactions with MTS reagents at this position are uninformative about any conformational change.

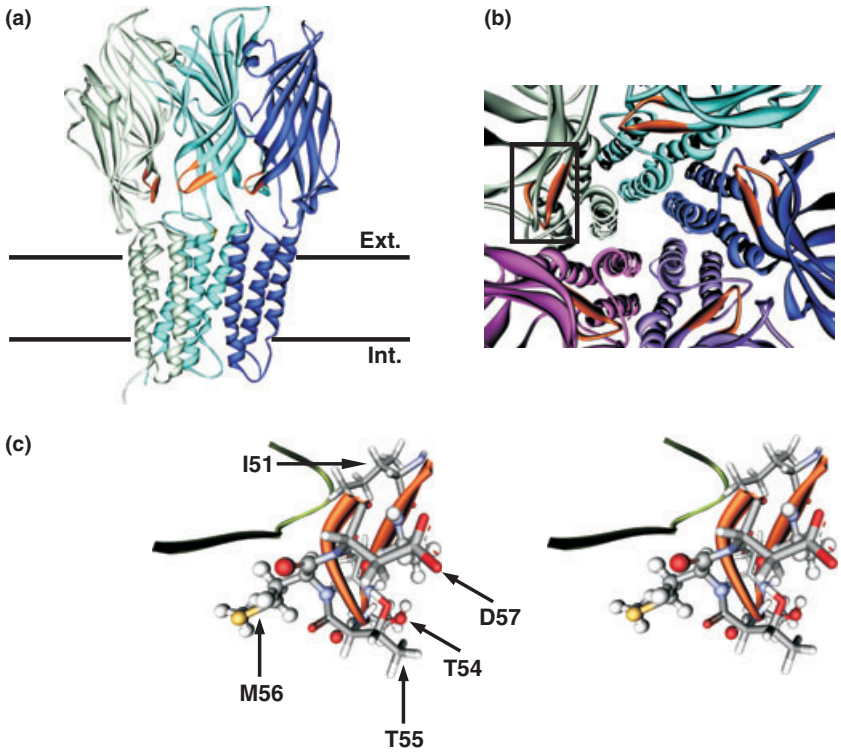

Fig. 8 GlyR homology model. (a) Side view of the GlyR as a ribbon with the two front subunits removed for clarity. Loop 2 (residues 51–57) is coloured brown. The innermost α-helix is the M2 domain connected to the M3 domain via the M2–M3 loop. The extracellular side is at the top and the intracellular side at the bottom. (b) The GlyR viewed from the extracellular side, looking down the pore, with loop 2 in brown and boxed. The apex of loop 2 is pointing anticlockwise. The five chains, (a–e), are coloured mint green, magenta, purple, dark blue and aqua, respectively. The pentamer is displayed as a perspective projection with a 50° angle. (c) Stereo view of the α-subunit loop 2 represented in the box in (b), looking towards the axis of the pore. Even-numbered residues are shown in ball-stick, odd-numbered residues in stick. The figure shows that the odd-numbered loop 2 residues with an increased EC_{50} when mutated to a cysteine does not all lie on the same side of the loop. It also shows that the residues accessible to MTS reagents have their side-chains pointing in different directions. The Cys-loop (dark green) is shown as a ribbon. The homology model shown is based on the prokaryotic ligand-gated ion channel from *Erwinia chrysanthemi* (ELIC) (Hilf and Dutzler 2008).

Relative conformational change

Since the publication of the AChBP crystal structure (Brejc *et al.* 2001), there has been considerable interest in the loop structures including loop 2 at the interface between the ECD and the transmembrane domain. It has been proposed that these loops provide a critical link in coupling the ligand-binding site and the top of the transmembrane domain (Miyazawa *et al.* 2003; Cederholm *et al.* 2009). Kinetic analysis of the naturally occurring mutant mouse *spasmodic* has demonstrated that the A52S substitution in loop 2 of the α1 GlyR impairs the transition to a pre-opening conformation of the receptor (Plested *et al.* 2007), supporting the idea of loop 2 being a link between ligand binding and channel opening. Our data corroborates this role of loop 2 in signal transduction and provides clear evidence for loop 2 undergoing a conformational change as part of this process. Voltage-clamp fluorometry has also inferred conformational changes in the α1 GlyR loop 2, however, recordings were made with the fluorophore covalently attached at a single position (A52C; Pless and Lynch 2009a,b). Our data provides state-dependent rates of MTS modification at three separate locations in loop 2 (A52C, T54C and M56C). It is more likely that this reflects a conformational change in loop 2, rather than simply a change in other structures around loop 2. Predictions of conformational changes in loop 2 have been made by comparing the α and non-α subunits from the *Torpedo* nAChR structure (Unwin *et al.* 2002; Unwin 2005) as well as comparisons of the prokaryotic ELIC and GLIC crystal structures (Bocquet *et al.* 2009). This is reflected in the changes in surface accessibility of some loop 2 residues between our homology models built with the ELIC and GLIC templates (Table 3) and the residues A52, T54 and M56 are among those that show a change. Thus, there is a concurrence between the structural predictions from ELIC/GLIC and the state-dependent rates of modification

described here for loop 2. This supports the usefulness of the prokaryotic ligand-gated ion channel structures in understanding the signal transduction process in ligand-gated channels.

Acknowledgements

The authors thank Ms. Kerrie Pierce for excellent technical assistance, Dr. Warren Kaplan for initial assistance with homology modelling and Dr. Jane Carland for critical reading of the manuscript. This work was supported by the National Health and Medical Research Council of Australia (Project Grants 230806 and 455310). N.L.A. was the recipient of an Australian Postgraduate Award.

Supporting information

Additional Supporting Information may be found in the online version of this article:

Appendix S1. Supplementary Material and Methods.

Figure S1. Alignments of the α1 glycine sequence with each subunit (a–e) from the three templates (*Torpedo marmorata*, *Erwinia chrysanthemi* and *Gloeobacter violaceus*) used in our homology modelling.

Figure S2. Examples of whole-cell currents from the cysteine substituted loop 2 residues.

As a service to our authors and readers, this journal provides supporting information supplied by the authors. Such materials are peer-reviewed and may be re-organized for online delivery, but are not copy-edited or typeset. Technical support issues arising from supporting information (other than missing files) should be addressed to the authors.

References

Absalom N. L., Lewis T. M., Kaplan W., Pierce K. D. and Schofield P. R. (2003) Role of charged residues in coupling ligand binding and channel activation in the extracellular domain of the glycine receptor. *J. Biol. Chem.* **278**, 50151–50157.

Betz H. (1990) Ligand-gated ion channels in the brain: the amino acid receptor superfamily. *Neuron* **5**, 383–392.

Bocquet N., Nury H., Baaden M., Le Poupon C., Changeux J. P., Delarue M. and Corringer P. J. (2009) X-ray structure of a pentameric ligand-gated ion channel in an apparently open conformation. *Nature* **457**, 111–114.

Bouzat C., Gumilar F., Spitzmaul G., Wang H. L., Rayes D., Hansen S. B., Taylor P. and Sine S. M. (2004) Coupling of agonist binding to channel gating in an ACh-binding protein linked to an ion channel. *Nature* **430**, 896–900.

Brejc K., van Dijk W. J., Klaassen R. V., Schuurmans M., van Der Oost J., Smit A. B. and Sixma T. K. (2001) Crystal structure of an ACh-binding protein reveals the ligand-binding domain of nicotinic receptors. *Nature* **411**, 269–276.

Cederholm J. M., Schofield P. R. and Lewis T. M. (2009) Gating mechanisms in Cys-loop receptors. *Eur. Biophys. J.* **39**, 37–49.

Colquhoun D. (1998) Binding, gating, affinity and efficacy: the interpretation of structure-activity relationships for agonists and of the effects of mutating receptors. *Br. J. Pharmacol.* **125**, 924–947.

Corringer P. J., Baaden M., Bocquet N., Delarue M., Dufresne V., Nury H., Prevost M. and Van Renterghem C. (2010) Atomic structure and dynamics of pentameric ligand-gated ion channels: new insight from bacterial homologues. *J. Physiol. (London)* **588**, 565–572.

Crawford D. K., Perkins D. I., Trudell J. R., Bertaccini E. J., Davies D. L. and Alkana R. L. (2008) Roles for loop 2 residues of α1 glycine receptors in agonist activation. *J. Biol. Chem.* **283**, 27698–27706.

Dellisanti C. D., Yao Y., Stroud J. C., Wang Z. Z. and Chen L. (2007) Crystal structure of the extracellular domain of nAChR α1 bound to α-bungarotoxin at 1.94 A resolution. [erratum appears in Nat. Neurosci. 2007 Sep;10(9):1222]. *Nat. Neurosci.* **10**, 953–962.

Dougherty D. A. and Lester H. A. (2001) Neurobiology. Snails, synapses and smokers. *Nature* **411**, 252–253, 255.

Guex N. and Peitsch M. C. (1997) SWISS-MODEL and the Swiss-PdbViewer: an environment for comparative protein modeling. *Electrophoresis* **18**, 2714–2723.

Hilf R. J. and Dutzler R. (2008) X-ray structure of a prokaryotic pentameric ligand-gated ion channel. *Nature* **452**, 375–379.

Hilf R. J. and Dutzler R. (2009) Structure of a potentially open state of a proton-activated pentameric ligand-gated ion channel. *Nature* **457**, 115–118.

Karlin A. and Akabas M. H. (1998) Substituted-cysteine accessibility method. *Methods Enzymol.* **293**, 123–145.

Kash T. L., Jenkins A., Kelley J. C., Trudell J. R. and Harrison N. L. (2003) Coupling of agonist binding to channel gating in the $GABA_{(A)}$ receptor. *Nature* **421**, 272–275.

Lee W. Y. and Sine S. M. (2005) Principal pathway coupling agonist binding to channel gating in nicotinic receptors. *Nature* **438**, 243–247.

Lester H. A., Dibas M. I., Dahan D. S., Leite J. F. and Dougherty D. A. (2004) Cys-loop receptors: new twists and turns. *Trends Neurosci.* **27**, 329–336.

Lynch J. W. (2004) Molecular structure and function of the glycine receptor chloride channel. *Physiol. Rev.* **84**, 1051–1095.

Lynch J. W., Han N. L., Haddrill J., Pierce K. D. and Schofield P. R. (2001) The surface accessibility of the glycine receptor M2–M3 loop is increased in the channel open state. *J. Neurosci.* **21**, 2589–2599.

McLaughlin J. T., Fu J. and Rosenberg R. L. (2007) Agonist-driven conformational changes in the inner β-sheet of α7 nicotinic receptors. *Mol. Pharmacol.* **71**, 1312–1318.

Miyazawa A., Fujiyoshi Y. and Unwin N. (2003) Structure and gating mechanism of the acetylcholine receptor pore. *Nature* **423**, 949–955.

Pascual J. M. and Karlin A. (1998) State-dependent accessibility and electrostatic potential in the channel of the acetylcholine receptor. Inferences from rates of reaction of thiosulfonates with substituted cysteines in the M2 segment of the alpha subunit. *J. Gen. Physiol.* **111**, 717–739.

Pless S. A. and Lynch J. W. (2009a) Distinct conformational changes in activated agonist-bound and agonist-free glycine receptor subunits. *J. Neurochem.* **108**, 1585–1594.

Pless S. A. and Lynch J. W. (2009b) Ligand-specific conformational changes in the α1 glycine receptor ligand-binding domain. *J. Biol. Chem.* **284**, 15847–15856.

Plested A. J., Groot-Kormelink P. J., Colquhoun D. and Sivilotti L. G. (2007) Single-channel study of the spasmodic mutation α1A52S in recombinant rat glycine receptors. *J. Physiol. (London)* **581**, 51–73.

Price K. L., Millen K. S. and Lummis S. C. (2007) Transducing agonist binding to channel gating involves different interactions in $5\text{-}HT_3$ and $GABA_C$ receptors. *J. Biol. Chem.* **282**, 25623–25630.

Reeves D. C., Jansen M., Bali M., Lemster T. and Akabas M. H. (2005) A role for the β1-β2 loop in the gating of 5-HT_3 receptors. *J. Neurosci.* **25**, 9358–9366.

Schwede T., Kopp J., Guex N. and Peitsch M. C. (2003) SWISS-MODEL: an automated protein homology-modeling server. *Nucleic Acids Res.* **31**, 3381–3385.

Unwin N. (1993) Nicotinic acetylcholine receptor at 9 A resolution. *J. Mol. Biol.* **229**, 1101–1124.

Unwin N. (2003) Structure and action of the nicotinic acetylcholine receptor explored by electron microscopy. *FEBS Lett.* **555**, 91–95.

Unwin N. (2005) Refined structure of the nicotinic acetylcholine receptor at 4A resolution. *J. Mol. Biol.* **346**, 967–989.

Unwin N., Miyazawa A., Li J. and Fujiyoshi Y. (2002) Activation of the nicotinic acetylcholine receptor involves a switch in conformation of the α subunits. *J. Mol. Biol.* **319**, 1165–1176.

Wang J., Lester H. A. and Dougherty D. A. (2007) Establishing an ion pair interaction in the homomeric ρ1 γ-aminobutyric acid type A receptor that contributes to the gating pathway. *J. Biol. Chem.* **282**, 26210–26216.